Organization of the magnetosphere during substorms

T. Živković[1,2] and K. Rypdal[1]

Received 26 May 2011; revised 15 February 2012; accepted 25 March 2012; published 5 May 2012.

[1] The change in degree of organization of the magnetosphere during substorms is investigated by analyzing various geomagnetic indices, as well as interplanetary magnetic field z-component and solar wind velocity x-component. We conclude that the magnetosphere self-organizes globally during substorms, but neither the magnetosphere nor the solar wind become more predictable in the course of a substorm. This conclusion is based on analysis of substorms in the period from 2000 to 2002. A minimal dynamic-stochastic model of the driven magnetosphere that reproduces many statistical features of substorm indices is discussed.

Citation: Živković, T., and K. Rypdal (2012), Organization of the magnetosphere during substorms, *J. Geophys. Res.*, *117*, A05212, doi:10.1029/2011JA016878.

1. Introduction

[2] The complexity of the magnetosphere has been extensively studied and one of its descriptions is based on the paradigm of self-organized criticality (SOC) coined by *Bak et al.* [1987]. Systems that exhibit SOC activate many degrees of freedom, their interactions are local, but due to the excitation of a scale-free hierarchy of avalanches when the system is slowly driven to a criticality threshold, long-range interactions develop, and the dynamics on different spatial and temporal scales is essentially the same. It has been shown that the magnetospheric-ionospheric system exhibit signatures characteristic of SOC-dynamics [*Vörös*, 1991; *Uritsky and Pudovkin*, 1998], and models for such description have been developed [*Valdivia et al.*, 2006; *Klimas et al.*, 2000; *Chapman et al.*, 1998; *Chang*, 1999; *Uritsky et al.*, 2002; *Kozelov and Kozelova*, 2003]. On the other hand, the magnetospheric-ionospheric system has also some signatures of intermittent turbulence [*Golovchanskaya et al.*, 2008], non-equilibrium phase-transitions [*Sitnov et al.*, 2001], as well as low-dimensional chaos [*Sharma et al.*, 1993]. It has been recently reported by *Živković and Rypdal* [2011] that the magnetosphere, interplanetary magnetic field (IMF) z-component B_z and solar wind flow speed v become more predictable and more persistent during magnetic storms, while only the magnetosphere reduces the effective number of degrees of freedom through self-organization. In that study the magnetosphere was studied through analysis of the geomagnetic indices SYM-H and D_{st}, since it is known that these indices respond to the intensification of the ring current during magnetic storms [*Wanliss and Showalter*, 2006]. In this article we analyze how different magnetospheric indices respond to the much more frequent and short-living events called substorms.

[3] Different geomagnetic indices represent different parts of the magnetosphere and respond to different dynamics. Geomagnetic indices studied in this article, are downloaded from World Data Center, with 1-min resolution. The most commonly used index for substorm studies is the auroral electrojet index (AE) defined as the difference between the AU index, which measures the strength of the eastward electrojet in the auroral zone, and the AL index, measuring the westward electrojet current, and is usually derived from 12 magnetometers positioned below the auroral oval [*Davies and Sugiura*, 1966]. We also use minute data for the IMF component B_z, as well as minute data for the solar wind velocity v_x component along the Sun-Earth axis. They are both retrieved from the OMNI satellite database where the data is time-shifted to the Earth's bow shock nose, and are given in GSE coordinate system. Intervals where data for B_z and v_x is missing are linearly interpolated.

[4] We have not analyzed other plasma parameters, since the plasma instruments can be influenced by solar X rays or energetic particle precipitation and are more unstable than the magnetometers. We also analyze the polar cap magnetic activity (PC), as well as the AU and the AL index. During magnetically disturbed times the westward electrojet, whose proxy is the AL index, increases abruptly due to currents from the magnetotail. On the other hand, the eastward electrojet, whose proxy is the AU index, increases due to the partial ring current closure via the ionosphere in the evening sector [*Feldstein et al.*, 2006]. Therefore, through the analysis of the AL and AU index we can get insight into the dynamics of different parts of the magnetosphere. The PC index monitors geomagnetic activity over the polar caps caused by changes in the IMF and the solar wind. This index is mostly influenced by field-aligned currents which flow at the poleward rim of the auroral oval, and is also sensitive to the ionospheric Hall currents in the polar cap [*Vennestrøm et al.*, 1991], which are particularly dominant in the summer

[1]Department of Physics and Technology, University of Tromsø, Tromsø, Norway.
[2]Swedish Institute of Space Physics, University of Uppsala, Uppsala, Sweden.

Corresponding Author: T. Živković, Swedish Institute of Space Physics, University of Uppsala, SE-75237 Uppsala, Sweden. (tatjana.zivkovic@irfu.se)

0148-0227/12/2011JA016878

time. Since field-aligned currents are closely related to the auroral electrojets, the linear correlation of the PC and AE indices is of the order of 0.8–0.9 in the winter and equinox for the Thule station on the northern hemisphere. The correlation is less in the summer due to the disturbance of the polar cap currents [*Vennestrøm et al.*, 1991]. Here we use the northern polar cap index measured at the Danish geomagnetic observatory in Thule (86.5°N).

[5] Magnetic substorms are associated with release and storage of energy and momentum from the solar wind to the magnetosphere. They consist of three phases. In the growth phase, typically lasting for about one hour, loading of the magnetic flux and energy into the magnetotail takes place. It is succeeded by the expansion phase (substorm onset), lasting 30–60 min, when hot plasma "unloads" earthward, leading to sudden brightenings of the polar aurora, and plasmoids are ejected away from Earth into the far tail. In the ionosphere, substorm onset is characterized by a rise of the westward electrojet current, which forms the substorm current surge with field aligned currents. The recovery phase returns the magnetosphere to its quiet state. The duration of this phase is 1–2 hours.

[6] Data about the times of substorm onsets are found in *Frey et al.* [2004], whose database is from the period between 2000 and 2002. These substorms were detected by the FUV instrument on the IMAGE spacecraft. Observations covered the peak of the last solar cycle. According to *Frey et al.* [2004] a substorm onset is only accepted as a separate event if at least 30 min have passed after the previous event. It is also required that local brightening of aurora occurs and that the aurora expands to the poleward boundary of the auroral oval and spreads azimuthally in local time for at least 20 min. The latter criterion excludes pseudo-breakups which do not develop into full substorms.

[7] The remainder of the paper is organized as follows: section 2 gives a brief overview of the methods used in the analysis of our data. Section 3 shows the results from application of these methods to the substorm data and section 4 is reserved for discussion.

2. Methods

2.1. Recurrence-Plot Analysis

[8] Recurrence-plot analysis was developed by *Eckmann et al.* [1987] and is very useful in studies of short and non-stationary time series. A comprehensive review of the method and its applications can be found in *Marwan et al.* [2007]. Substorm durations are at most a few hours and all indices show non-stationary behavior during the events. Recurrence-plot analysis is very suitable for handling such short non-stationary time series. The method is useful for low-dimensional deterministic dynamical systems as well as for high-dimensional systems and for stochastic signals. It can also provide useful information about non-autonomous systems. An impression of the versatility of this technique can be obtained from *Marwan et al.* [2008]. For low-dimensional systems

$$\frac{d\mathbf{z}}{dt} = \mathbf{f}[\mathbf{z}(t), t], \tag{1}$$

recurrence plots are based on the recurrences of a trajectory $\mathbf{z}(t)$ on the d-dimensional attractor in a $p > d$-dimensional phase space. If the system is autonomous, i.e. no explicit time dependence of the phase-space flow $\mathbf{f}[\mathbf{z}]$, and if the attractor of trajectory has dimension d, Takens' time delay method [*Takens*, 1981] can be used to construct an $m > 2d$-dimensional embedding space on which the attractor can be mapped continuously and one-to-one. The embedding space is constructed from the time series $x_i = g(\mathbf{z}[i\delta t])$, where $g(\mathbf{z})$ is the measurement function. Here $t = i\delta t$, and δt is the sampling time of the time series. The mapping is given by

$$\mathbf{x}_i = \left(x_i, x_{i+\tau}, \ldots, x_{i+(m-1)\tau}\right), \tag{2}$$

where τ is the time delay. There are practical constraints on useful choices of the time delay τ. If τ is much smaller than the autocorrelation time the image of the attractor in the embedding space becomes essentially one-dimensional. If τ is much larger than the autocorrelation time, noise may destroy the deterministic connection between the components of $\mathbf{x}(t)$, such that our assumption that $\mathbf{z}(t)$ determines $\mathbf{x}(t)$ will fail in practice. A common choice of τ has been the first minimum of the autocorrelation function, but it has been shown that better results are achieved by selecting the time delay as the first minimum in the average mutual information function [*Abarbanel*, 1996], which we also use in this article.

[9] The recurrence-plot analysis deals with the trajectories in the embedding space. If the original time series $x(t)$ has N elements and a time delay τ, we have a time series of $N - (m-1)\tau$ vectors $\mathbf{x}(t)$ for $t = 1, \ldots, N - (m-1)\tau$. This time series constitutes the trajectory in the reconstructed embedding space.

[10] The next step is to construct a $N - (m-1)\tau \times N - (m-1)\tau$ matrix $R_{i,j}$ consisting of elements 0 and 1. The matrix element (i, j) is 1 if the distance is $\|\mathbf{x}_i - \mathbf{x}_j\| \leq \epsilon$ in the reconstructed space, and otherwise it is 0. The recurrence plot is simply a plot where the points (i, j) for which the corresponding matrix element is 1 is marked by a dot. For a deterministic system the radius ϵ is typically chosen as small fraction of the diameter of the reconstructed attractor, but varies for different sets of data. In our analysis we have used 10% of the total extent of the set spanned by the trajectory analyzed in the embedding space. This is a rule of the thumb generally accepted in the recurrence-plot literature [*Marwan et al.*, 2007]. The results are not very sensitive to this choice, but issues arise if ϵ is too large (to crude resolution and practically no information) or too small (poor statistics).

[11] Dynamical systems with a large number of independent or weakly dependent degrees of freedom can only be described either by large-scale numerical simulation or by stochastic methods. For such systems the phase-space attractor is also high-dimensional and cannot be mapped one-to-one onto a low-dimensional time delay embedding space. Nevertheless, the evolution of the "projection" of the phase-space vector onto the embedding space usually provides valuable information if the measurement function is carefully chosen to be sensitive to variation of those degrees of freedom that are in the focus of our interest (for instance we should use the AE index rather than the D_{st} index as measurement function if substorm activity is studied). Some of this information can be discerned from the recurrence plots, even if the recurring states are not recurrences of the full phase-space vector, but only of the projections. This is true also if the full set of differential equations is non-

autonomous [*Webber and Zbilut*, 1994]. The time-dependent forcing invalidates the embedding theorem, but we are not assuming a perfect embedding anyway. We just have to be aware that dynamical features we observe in the recurrence plot may well reflect the dynamics of the forcing and not only the internal dynamics of the unforced system.

[12] Of particular interest is the analysis based on the diagonal line structures of the recurrence plots [see, e.g., *Trulla et al.*, 1996]. If the projected trajectory has a tendency to repeat its path when it recurs to the same region in embedding space, recurrences tend to be localized along unbroken diagonal segments. The longer these segments are, the more predictable is the path. We define the average inverse diagonal line segment length Γ:

$$\Gamma \equiv \langle l^{-1} \rangle = \sum_l l^{-1} P(l) / \sum_l P(l), \tag{3}$$

where $P(l)$ is a histogram over diagonal lengths:

$$P(l) = \sum_{i,j=1}^{N} \left(1 - R_{i-1,j-1}\right)\left(1 - R_{i+l,j+l}\right) \prod_{k=0}^{l-1} R_{i+k,j+k}. \tag{4}$$

[13] It was shown heuristically in *Živković and Rypdal* [2011] that Γ can be used as a proxy for the largest Lyapunov exponent in deterministic systems and as a measure of persistence in stochastic systems. For a deterministic system we demonstrated the connection with the largest Lyapunov exponent λ by computing λ and Γ along a period-doubling route to chaos for the Lorenz system. By computing Γ and the self-similarity exponent h for numerically generated fractional Brownian motions (fBm) with h in the range $0 < h < 1$ we established the relation $\Gamma = 0.72 - 0.57h$ in the range of persistent Brownian motions ($0.5 < h < 1$). An fBm is a Gaussian stochastic process $\{x(t)\}$ which satisfies the self-similarity condition $x(t) \stackrel{d}{=} \lambda^{-h} x(\lambda t)$ for all λ. Here $\stackrel{d}{=}$ denotes identity in distribution. For a given time series h can be estimated from the variogram [*Živković and Rypdal*, 2011]. For a chaotic, deterministic system, the inverse of the largest Lyapunov exponent is a measure of predictability. For a persistent stochastic process h is also such a measure, and Γ decreases with increasing h. Thus we suggest to use the inverse of Γ as a measure of predictability. Since signals of interest are a mixture of deterministic and stochastic components, and many stochastic processes are neither self-similar nor Gaussian, we do not consider Γ as an absolute measure of predictability, but when a decrease of Γ takes place in a time series under certain conditions, e.g. during a magnetic storm, we interpret this as an increase in predictability of the dynamics under these conditions.

[14] We compute Γ for embedding dimension $m = 1$. An obvious advantage of this choice is that we don't have to worry about the choice of time delay τ. A higher value of m does not make much more sense since the dynamics of the magnetosphere and the solar wind is strongly influenced by a high-dimensional/stochastic component and cannot be unfolded in any higher-dimensional embedding space. Also, if the embedding dimension is inappropriately high, spurious long diagonal lines will appear in the recurrence plot. Moreover, the way Γ depends on other predictability measures like Lyapunov exponent or self-similarity exponent is rather insensitive to the choice of m, hence Γ can be used to detect changes in predictability irrespective of the choice of embedding dimension.

2.2. A Test for Determinism

[15] We shall adopt a terminology where a physical system is deterministic if it can be described as a low-dimensional dynamical system, i.e. by the autonomous version of equation (1). A test of determinism was developed by *Kaplan and Glass* [1992, 1993] which takes advantage of the fact that the trajectory through a given position in phase space is completely determined by this position, and if a trajectory recurs to the vicinity of this point the tangents of the trajectory in these two points are approximately parallel. This is in contrast to a stochastic system, where the directions of the tangents are independent for the two points. Let us assume that the phase space is divided into boxes. In our test, a box size is chosen as the average distance a phase-space point moves in the m-dimensional embedding space during one time step. The displacement of the trajectory inside a box, in m-dimensional phase space is given from the time delay embedding reconstruction:

$$\begin{aligned}\Delta\mathbf{x}(t) = \big[&x(t+b) - x(t), x(t+\tau+b) - x(t+\tau), \ldots, \\ &x(t+(m-1)\tau+b) - x(t+(m-1)\tau)\big],\end{aligned} \tag{5}$$

where b is the characteristic time the trajectory spends inside a box. The tangent for the kth pass through box j is the unit vector $\mathbf{u}_{k,j} = \Delta\mathbf{x}_{k,j}(t)/|\Delta\mathbf{x}_{k,j}(t)|$. The averaged tangent in the box is

$$\mathbf{V}_j = \frac{1}{n_j} \sum_{k=1}^{n_j} \mathbf{u}_{k,j}, \tag{6}$$

where n_j is the number of passes of the trajectory through box j. In the case of deterministic dynamics and finite box size, $\mathbf{V}_j$ will not depend very much on the number of passes n_j, and V_j will converge to 1. In contrast, for the trajectory of a random process with independent increments, V_j will decrease with n_j as $V_j \sim n_j^{-1/2}$. Thus, to obtain better statistics for the description of average tangents we compute the average V_j as a function of the number of passes through a box:

$$L_n \equiv \langle V_j \rangle_{n_j = n}, \tag{7}$$

where this average is done over all boxes with same number n_j of trajectory passes.

[16] There are obvious similarities between this test for determinism and the one for predictability developed in the previous subsection. Both measure the degree of divergence of projected trajectories starting at almost the same position in the reduced embedding space. In those cases when the system can be described as a low-dimensional dynamical system (equation (1) without the explicit time dependence in the flow field), we have $L_n = 1$ for all n, provided the embedding dimension m is sufficiently large to unfold the attractor. In this case Γ will reflect the magnitude of the largest Lyapunov exponent, and the two tests clearly measure different properties. For a stochastic process L_n is independent of m [*Živković and Rypdal*, 2011] and independent of its persistence, which is easily demonstrated by

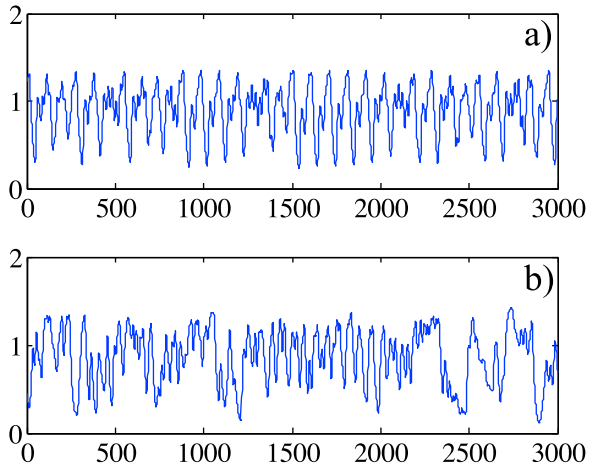

Figure 1. Time series for the MG equation: (a) $\delta = 30$ and (b) $\delta = 150$.

computing it for fBms with varying self-similarity exponents h. However, for the systems considered in this paper the signals contain both a deterministic and a stochastic component. In this case the phase-space trajectory cannot be mapped one-to-one onto the embedding space for any choice of m, and the distinction between the two methods is less clear. One could envisage that an increase of the low-dimensional (deterministic) component relative to the stochastic one could enhance both L_n and Γ^{-1}. On the other hand, an increase in predictability in either the deterministic or the stochastic component, without change in relative strength of the two components, could also influence both measures. Thus, in those cases where both measures either increase or decrease together, it is difficult to decide whether the cause is a change in determinism or in predictability. However, in situations when only one of the measures undergoes a change, or they change in opposite direction, the interpretation is unambiguous.

[17] *Kaplan and Glass* [1992, 1993] also suggest another test of determinism, which does not suffer from this ambiguity. It takes advantage of how the measure of determinism, the curves of L_n versus n, changes when we construct a new surrogate time series for which the effect of nonlinearity in a low-dimensional system has been corrupted. This surrogate signal has the same power spectral density (and hence same auto-covariance) as the original signal, but the phases of the Fourier coefficients have been randomized. From application of this procedure to synthetic stochastic and low-dimensional signals we have gained support for the conjecture that randomization of phases do not change these curves for neither stochastic or high-dimensional, nor low-dimensional, linear systems. Only for low-dimensional, nonlinear systems will the surrogate data curves lie below those based on the original data. These features were demonstrated for numerical solutions of the Lorenz system (low-dimensional, nonlinear and chaotic) in *Živković and Rypdal* [2011]. Here we demonstrate the same for L_n versus n for the Mackey-Glass (MG) equation [*Mackey and Glass*, 1977]:

$$\frac{dx}{dt} = -lx(t) + a\frac{x(t-\delta)}{1+x(t-\delta)^c}. \tag{8}$$

Unlike the Lorenz system, the attractor of this system is in general high-dimensional. However, for some set of parameters, e.g. $a = 0.2$, $l = 0.1$, $\delta = 30$, $c = 10$, the attractor of MG dynamics can be low-dimensional and L_n derived from the MG equation will fall more slowly with increasing n than that for the randomized version, as shown in Figure 2a. The time series for these parameters is plotted in Figure 1a. In order to calculate L_n, embedding dimension $m = 8$, $\tau = 15$, and $b = 1$ are used. Here we compute and plot mean L_n for ten realizations of the MG equation and for ten realizations with phases of the Fourier coefficients randomized. Standard deviation is not plotted since it is of the same order as the symbol size. For a discussion of how we treat errors and statistical significance in this paper, see section 2.3. It has been shown in *Mackey and Glass* [1977] that the dimension of the attractor for the dynamics of MG equation increases with δ. Therefore, we compute mean L_n as a function of n when $\delta = 150$. Figure 1b shows this time series, while mean L_n versus n is shown in Figure 2b. Unlike in Figure 2a, where

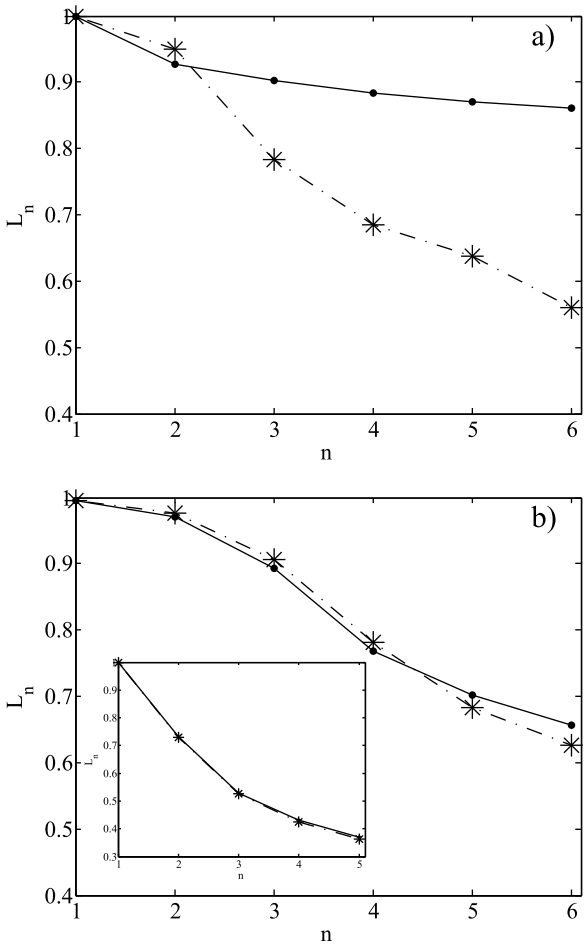

Figure 2. Vector length L_n versus number of passages n averaged over an ensemble of 10 realizations: bullets are derived from numerical solutions to the MG equation, stars are derived from these solutions after randomization of phases of Fourier coefficients: (a) $\delta = 30$ and (b) $\delta = 150$. Inset shows same characteristics for the O-U process. The error bars are of the same order as the symbol size.

L_n of the original and randomized time series are clearly separated, in Figure 2b L_n for the original and randomized time series are overlapping, demonstrating that the high-dimensional attractor diminishes the difference in mean L_n between the original and randomized time series. Here, m = 10, τ = 15, and b = 2 is used. The inset in the same figure shows the same results for a Ornstein-Uhlenbeck (O-U) stochastic process. The stochastic equation used to generate such a process was described in *Živković and Rypdal* [2011]. The coefficients in this equation are generated from fitting the variogram of the numerically generated process to the variogram of the AE index by means of least squares regression (for definition of the variogram see *Živković and Rypdal* [2011, equation (12)]). In O-U equation, the embedding dimension used is m = 8, τ = 15, and b = 1. L_n for the MG equation when δ = 150 falls more slowly as a function of n than that for the O-U process, since the latter is stochastic infinite dimensional process. The parameter b is chosen such that a sufficient number of trajectories pass through the phase-space box to make a good statistics up to n = 6. Realizations of a stochastic process like the O-U is indistinguishable from realizations of a measurement function of a high-dimensional deterministic system for which the embedding dimension is too small to unfold the attractor. The L_n-curve for the O-U process is unchanged after randomization of phases and shows that this test for determinism is negative for stochastic (and high-dimensional) systems. We have verified that this is the case also for strongly persistent (highly predictable) O-U processes. This is completely reasonable on theoretical grounds; the long-range persistence in an fBm only depends on the predominance of low frequencies in the power spectrum, not on correlation between the phases of the Fourier coefficients. Thus, this test is not measuring predictability and is a useful test for detecting changes in determinism in time series.

2.3. Statistical Errors and Significance

[18] The plots presented in Figure 2 are based on computation of a measure of determinism (L_n) for individual numerical realizations of a signal generated by two particular models. In the following we shall denote such a realization as a *sample* of the ensemble of signals. In the same figure we also present plots based on computation of this measure from signals with randomized phases of Fourier coefficients (here denoted surrogate data). In an ensemble of such samples of the signal this measure has a Gaussian statistical distribution with standard deviation σ_S. The purpose of computing these measures is to reveal a statistically significant difference between the measures of original data and the surrogate data. For the MG signal for δ = 30 (Figure 2a) the separation between the two curves is obviously significant, while for δ = 150 and for the O-U process (Figure 2b) it is obviously not. However, in section 3 we will perform many estimates of similar nature, where the curves are separated, but where we have to address the question whether this separation is statistically significant. A common situation is that the standard deviation σ_S is of the same order as the difference between the computed measure for the original data and the surrogate data, so a statistically significant separation of the measures cannot be established from estimation of the measure for only one sample of each data set. However, the statistical distribution of the ensemble mean computed by averaging over N independent samples is $\sigma = \sigma_S/\sqrt{N}$. What we have plotted in Figure 2 is this ensemble mean, and the uncertainty in this estimate is therefore σ (not σ_S) and σ should be quoted as the error bar of this estimate.

[19] In section 3 we compute measures from various geomagnetic indices for ensembles of N sample data sets. In all these cases we are able to choose N so large that the error bars for the ensemble means become of the same order as the symbol size in the plots. Plotting the error bars will make it difficult to recognize the different symbols and is the reason why none of the figures in that section will be equipped with error bars.

[20] The errors discussed so far refers to statistical uncertainty, which can always be improved with more data. This should not be confused with systematic errors, which can have many sources. One such source is non-stationarity of the observational time series. Others are related to inadequacies in the definition and computation of measures of predictability and determinism.

3. Results

[21] In *Rypdal and Rypdal* [2010] it was shown that the fluctuation amplitude (or more precisely; the one-timestep increment) $\Delta y(t)$ of the AE index is on the average proportional to the instantaneous value $y(t)$ of the index. This gives rise to a special kind of intermittency associated with multiplicative noises, and leads to a non-stationary time series of increments. However, the time series $\Delta y(t)/y(t)$ is stationary, implying that the stochastic process $x(t) = \log y(t)$ has stationary increments. Thus, a signal with stationary increments, which still can exhibit a multifractal intermittency, can be constructed by considering the logarithm of the AE index. We use transformed versions of geomagnetic indices: tAE = log(AE), tAL = log(0.1928 |AL| + 10.50), tAU = log(0.1167 |AU| + 13.50), tPC = log(0.0503 |PC| + 0.1978), while B_z and v_x have increments which are not strongly dependent on their magnitude, and do not need transformation to obtain stationary increments.

[22] It is well known that the AE index exhibits scale-free characteristics which often is associated with stochastic dynamics since its power spectral density has two distinct power law regimes [*Tsurutani et al.*, 1990]. However, it has also been shown that apart from colored noise which dominates the dynamics of the AE index on timescales up to 100 min, there are also signatures of low-dimensional, chaotic characteristics as well [*Athanasiu and Pavlos*, 2001]. These properties will be discerned from the analysis of determinism of geomagnetic indices in section 3.2.

3.1. Predictability Analysis

[23] First, we discuss two magnetic substorms that occurred on September 8th, 2002. The first substorm onset was registered at 5:01 UT and the other at 21:26 UT. The second substorm onset started after 13 hours of northward IMF B_z. In Figure 3a the transition between dark and white bands in the recurrence plot indicates changes in the dynamics in the tAE. The first transition marked by an arrow occurs around the first substorm onset. The next appears at the onset of the second substorm. For instance, the broad white band in Figure 3a corresponding to $i > 300$, $j < 300$ indicates that a region in embedding space visited before the

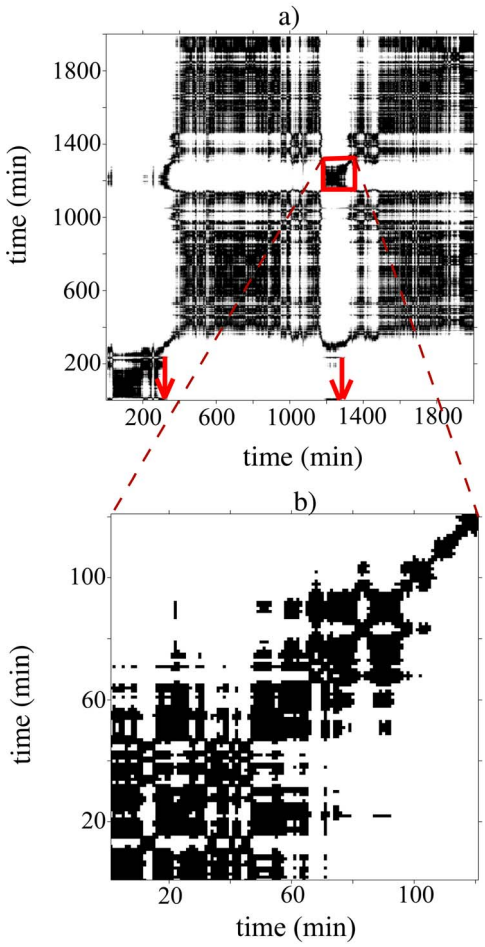

Figure 3. Recurrence plots for tAE: (a) For the entire day of September 8th, 2002, containing two distinct substorms whose onsets are marked by arrows. (b) Blow-up of recurrence plot for second substorm (marked by square in Figure 3a).

substorm onset is never visited after onset. Figure 3b contains a blow-up of the recurrence plot for the second substorm. The image pales away from the main diagonal, which indicates that the process is non-stationary due to the intensification and the movement of ionospheric currents during the substorm. Since the plot pattern changes during the substorm we might expect that Γ, which is defined from the diagonal lines of the plot, will change as well.

[24] We obtain Γ for tAE, tAU, tPC, tAL, B_z, and v_x for substorms whose onsets were taken from the database of *Frey et al.* [2004]. The variation of Γ over a 6 hour time interval, three hours before and three hours after the substorm onset, is computed from recurrence plots derived from thirty-minute windows so that 11 Γ-values are obtained for each substorm. Substorms with onsets separated by less than 3 hours are discarded from the ensemble to avoid overlap. Thus 1922 "independent" substorms are included in the ensemble.

[25] The time evolution of Γ is computed for these substorms and averaged. The results are presented in Figure 4a. Apparently, there is no significant variation of the ensemble average of Γ over the duration of a substorm for any of the geomagnetic indices.

[26] On timescales less than 100 min all quantities analyzed can be modeled as non-stationary multifractal motions whose persistence can be characterized by an exponent h [*Rypdal and Rypdal*, 2010, 2011]. Increasing h implies higher persistence and predictability, corresponding to a reduction of Γ. We compute h from the variogram [*Živković and Rypdal*, 2011, equation (12)]. Figure 4b shows no variation in ensemble mean of 2 h for any of the indices, confirming the result obtained for Γ. Further, the same procedure is repeated for all indices during the entire year 2000, 2001 and 2002. In this case, each set is computed over 6 hour time intervals, without distinguishing between substorm and quiet times. The result (not shown here)is that the ensemble average of Γ and 2 h overlaps with the results presented in Figure 4, hence that the predictability and persistence do not change significantly during substorms.

[27] The same analysis is done for B_z and v_x. Mean values for Γ and 2 h are plotted in Figure 5, showing no significant change of predictability during substorms for the solar wind observables. Values for these parameters during all times overlap with the results in Figure 5, as in the case for the geomagnetic indices. The example of two substorms from September, 8th, 2002 shows a reduction of Γ in tAE around substorm onset (not shown here), but this day seems to be an exception rather than the rule.

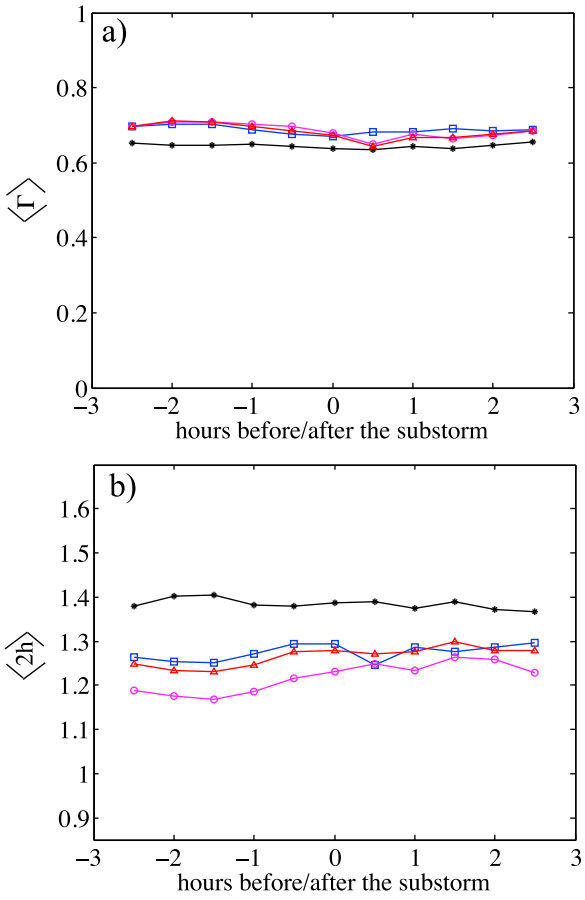

Figure 4. (a) ⟨Γ⟩, obtained by averaging Γ over the substorm ensemble. (b) Ensemble means ⟨2 h⟩. Triangles represent tAE, squares tAU, stars tPC, and circles tAL. The standard errors for all points are in the range $0.003 < \sigma < 0.02$.

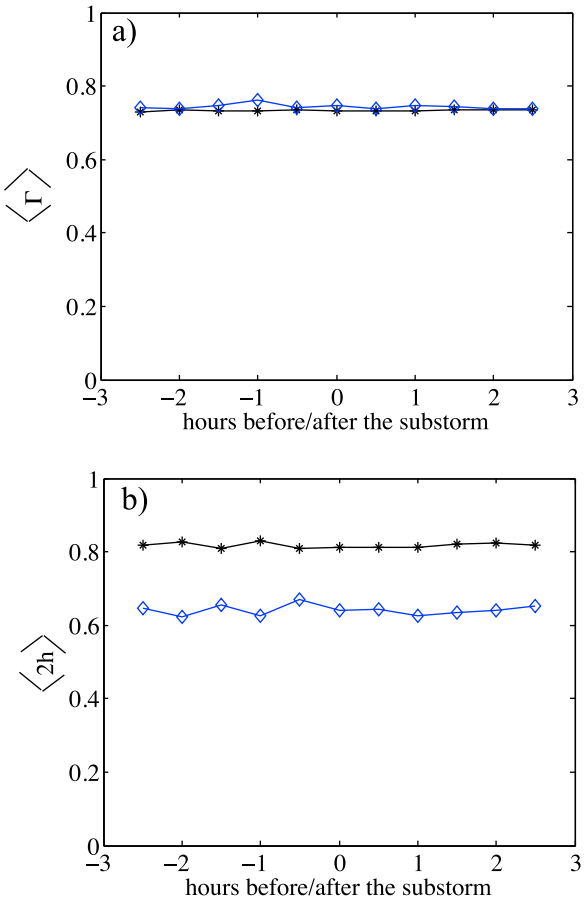

Figure 5. (a) $\langle\Gamma\rangle$, obtained by averaging Γ over the substorm ensemble. (b) Ensemble means $\langle 2h\rangle$. Stars represent B_z and diamonds v_x. Standard error for $\langle\Gamma\rangle$ is of the order $\sigma \approx 0.02$, while for $\langle 2h\rangle$ it is $\sigma \approx 0.04$.

3.2. Determinism Analysis

[28] The signals we study are dominated by a stochastic component and their L_n decreases when number of passes n is increased. However, the existence of a low-dimensional component in e.g. the tAE can be demonstrated by computing L_n and then do the same for the surrogate signals obtained by randomizing phases of Fourier coefficients. For computation of mean L_n, we use AE index data from the years 2000, 2001 and 2002. Each sample value of L_n is computed over a record of 7200 points, while the ensemble mean L_n is computed by averaging over ensembles of 9, 15 and 14 realizations, respectively. The number of realizations nn in the ensemble depends on the number of substorms in the respective years and is obtained as nn = (*number of substorms*) · 150/7200, since the length of a substorm will be 150 min, and one sample L_n is calculated over 7200 points.

[29] The same number of realizations is used to compute L_n for randomized time series as well. Here, ensemble mean of L_n is computed over both substorm and quiet periods to which we refer as all data. We have also computed mean L_n for several other record lengths, but the value does not change significantly. The embedding dimension is m = 8, and τ = 10 minutes. The sample values of L_n are statistically independent and Gaussian distributed with standard deviation σ_s, and hence the standard error of the ensemble mean is $\sigma_s/\sqrt{nn}$, where nn is the number of realizations. This error is for all L_n-curves shown in this paper of the same order as the symbol size, and is therefore not shown explicitly in the figures. As observed in Figure 6a, where triangles are for the all data, and stars are for randomized data, L_n for tAE is higher than for the randomized version, indicating existence of a low-dimensional and nonlinear component in the signal. The same is shown for tAU, tAL, and tPC indices in Figures 6b and 7, respectively. Notice that for the O-U process in the inset of Figure 2b, L_n for the randomized version is overlapping with the L_n of the O-U process itself.

[30] Also, the same test was done for the geomagnetic index SYM-H in *Živković and Rypdal* [2011], and even though analysis of this index yields low-dimensionality during magnetic storms, L_n is indistinguishable from its randomized version when averaged over a year, where both storm and quiet times are taken into account. Further, L_n computed for B_z and v_x (triangles) is indistinguishable from the L_n of their randomized versions (stars), as is shown in Figure 8.

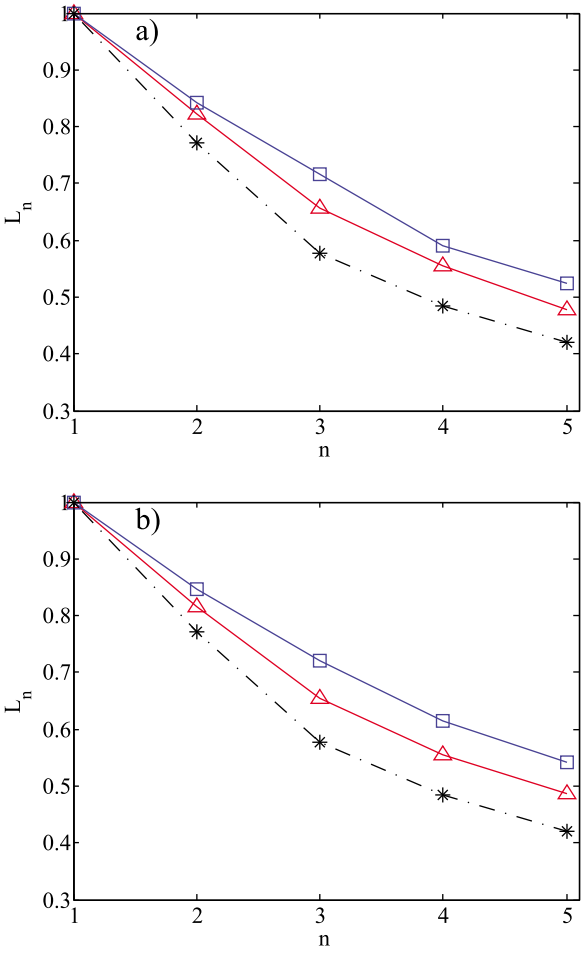

Figure 6. L_n averaged over an ensemble of realizations (for explanation see the main text); squares are derived during substorms, triangles from all data, stars from all data after randomization of phases of the Fourier coefficients, (a) for tAE and (b) for tAU. Standard errors are of the same order as the symbol size.

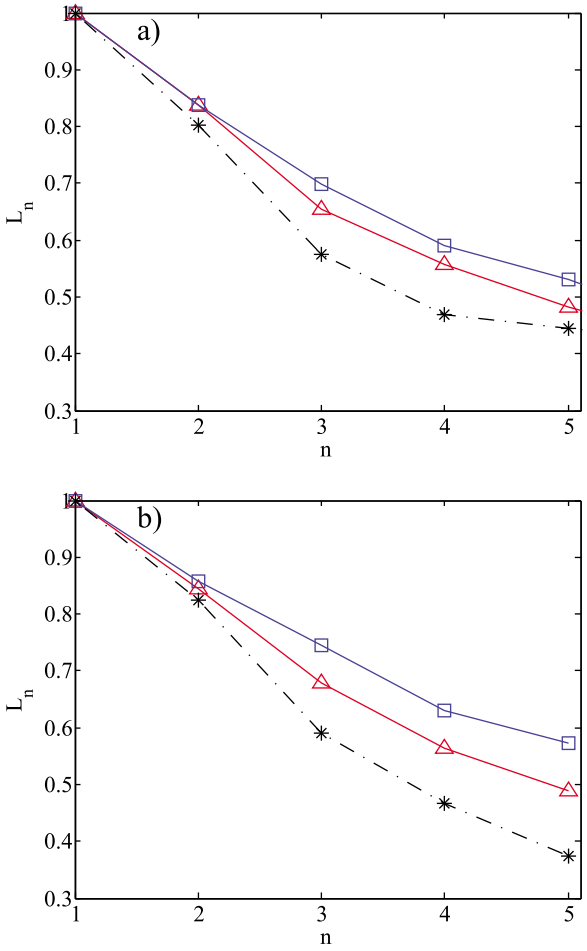

Figure 7. L_n averaged over an ensemble of realizations; squares are derived during substorms, triangles from all data, stars from all data after randomization of phases of the Fourier coefficients, (a) for tAL and (b) for tPC. Standard errors are of the same order as the symbol size.

[31] As we demonstrate below tAE, tAU and tPC all exhibit a discernible low-dimensional component during substorms. Since substorms occur very often, sometimes several per day, this low-dimensionality is discernible also when averaged over both substorm and quiet period data, as already shown. We use the substorm database and compute L_n in the time interval 1 hour before and 1.5 hours after the substorm onset. This way we generally include all phases of the substorm. Substorms with onsets separated by less than 3 hours are discarded from the ensemble to avoid overlap, as already mentioned in the previous section.

[32] It was shown in *Živković and Rypdal* [2011] that increasing the embedding dimension will result in a better estimate for the determinism L_n for systems with low-dimensional dynamical component, while no change in determinism can be seen for a stochastic signal like the O-U process. Therefore, in principle one should use as high embedding dimension as possible. However, as shown below, increasing embedding dimension reduces the number of data points available in the embedding space, and hence the statistical uncertainty in the estimates increases. Thus, a compromise must be found in each case. Ideally τ should be chosen to correspond to the first minimum of the average mutual information (which is $\tau \approx 20$ in most of our data). However, in our data we are limited by the length of the time records, which is the typical length of a substorm. We use records of length 2.5 hours (record length $L = 150$ data points), chose $\tau = 10$ minutes, and $m = 8$ (when $\tau = 20$, results are the same, but due to better statistics, we use $\tau = 10$). This leaves a trajectory record in embedding space of length $N - (m-1)\tau = 80$ (from equation (2)). These 80 data points are not sufficient to produce meaningful estimates for L_n, hence we compute one value of L_n by means of a string of 7200 data points (as in the case for "all" and "randomized" data), comprising $7200/150 = 48$ successive substorms. From such a string we can compute an L_n which should be perceived as an average evolution characterizing those 48 substorms, and we consider it to represent one sample value of the L_n-evolution of the substorm process. Further, mean L_n values are computed over an ensemble of 9, 15 and 14 realizations for the year 2000, 2001 and 2002, respectively, and for each year the standard error of the mean σ is estimated. This analysis is made for tAE, tAL, tAU, and tPC, and compared to L_n computed from all data where the mean L_n is

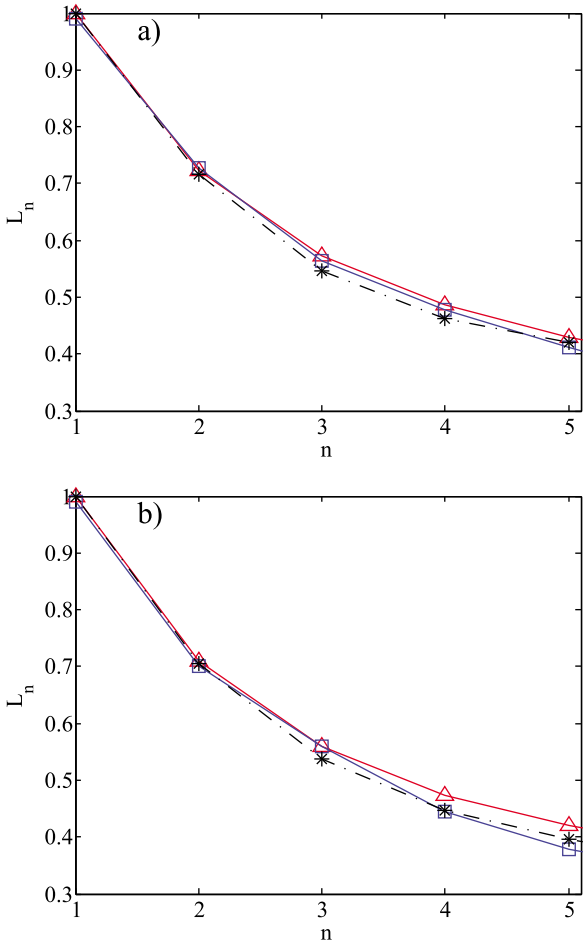

Figure 8. L_n averaged over an ensemble of realizations; squares are derived during substorms, triangles from all data, stars from all data after randomization of phases of the Fourier coefficients, (a) for B_z and (b) for v_x. Standard errors are of the same order as the symbol size.

calculated over the same number of realizations as for the substorm data. Figures 6 and 7 are plotted for the year 2000 and illustrate that all geomagnetic indices (except tAL) exhibit elevated determinism during substorm times (squares) in respect to all data (triangles), i.e. low-dimensionality increases during substorms. Future studies should investigate why determinism in tAL index change very little during magnetospheric substorms. Notice that if we could obtain equally good statistics with higher embedding dimension, it would be very likely that the determinism during substorms would be even more elevated than it is for $m = 8$. Also, we believe that L_n during substorms would be more elevated over L_n that would be computed from data where all substorms are excluded. However, this is difficult to do in practice, since quiet intervals between substorms have very unequal lengths. Mean L_n during substorms in 2001 and 2002 is also elevated over L_n computed for all data in 2001 and 2002, but the elevation is slightly smaller. L_n for the geomagnetic indices plotted in Figures 6 and 7, is obtained for $b = 1$. Box size of $b = 2$ gives very similar results, but larger boxes include more trajectories and the difference between determinism during substorms and all the data tend to decrease. As we see in the above analysis, L_n versus n looks similar to an O-U process, demonstrating that geomagnetic indices reveal predominantly stochastic dynamics. However, L_n for the original (either all or substorm times) is elevated over the L_n for the randomized time series, indicating that there is also a low dimensional, nonlinear component present in the time series.

[33] Another way to demonstrate the existence of a low-dimensional component in these indices is to compare the determinism computed from the tAE during substorms with signals generated numerically from the O-U equation, whose coefficients are fitted to the tAE under substorm through least squares regression procedure. For each of a large number of realizations of the O-U process, we compute the ensemble mean of L_4 as a measure of low-dimensionality, for embedding dimension $m = 8$ and $\tau = 20$. The choice of L_4 from the L_n versus n curve is a compromise between clear separation between low-dimensional and stochastic dynamics and small error bars (which increase with increasing n). The ensemble mean for O-U process is $L_4 \approx 0.40$, while for deterministic process $L_4 \sim 1$. In contrast, Figure 6a shows that $L_4 \approx 0.60$ for tAE under substorm conditions, which gives a clear indication that the AE index is neither fully deterministic nor stochastic.

[34] In Figure 8 we plot L_n for B_z and v_x, also when $b = 1$, and observe no increase in determinism during substorms. This indicates that the increased low-dimensional component in the geomagnetic indices during substorms is not imposed on the magnetosphere by the growth of such a component in the solar wind. In other words: the organization of the magnetosphere during substorms is a *self*-organization.

4. Discussion

[35] We have applied recurrence-plot analysis and a test of determinism to geomagnetic indices AE, AU, AL and PC, as well as IMF B_z and solar wind velocity x- component v_x. Recurrence plots were applied by *March et al.* [2005a] to connect solar wind observables to the AL and AU indices, concluding that the correlation between these indices results from magnetic storm signatures appearing in both time series. Also, correlation between the solar wind electric field v_xB_z and the AE index was studied in *March et al.* [2005b], invoking mutual information. Here it was found that correlation is present intermittently on the timescales of a few hours, suggesting that substorms are information carriers between the solar wind and the magnetosphere. In our study, recurrence analysis is used to measure the inverse average diagonal line length Γ which is heuristically shown to be a useful measure of predictability of the dynamics. As an alternative predictability measure the self-similarity exponent h was measured during the course of substorms. No systematic variation of h or Γ during substorms has been detected in an ensemble of all substorms in the period from 2000–2002. This is true both for geomagnetic indices and the solar wind observables. Thus we conclude that geomagnetic indices which represent dynamics in the magnetotail, plasma sheet boundary layer, partial ring current, and polar cap convection, do not become more predictable during substorms. The same applies for observables representing the dynamical state of the solar wind driver. From the analysis of a spatiotemporal dynamical model of the high latitude magnetic perturbation, it was shown in *Valdivia et al.* [1999] that the nonlinear dynamical model for the evolution of the spatial structure produces better prediction than the linear one during intense magnetospheric activity. In this article, a simple test for determinism has shown as well that the AE index exhibits some nonlinear characteristics, but in addition, it has a weak low-dimensional component. These characteristics are elevated during substorms, as is illustrated in Figure 6a. Other geomagnetic indices (to a lesser extent AL index) also show same signatures during magnetic substorms (see Figures 6b and 7), which could indicate that the magnetosphere develops low-dimensional dynamics under substorm conditions. For the AE index similar results were obtained by *Athanasiu and Pavlos* [2001], who applied singular value decomposition (SVD) analysis to the AE index. They concluded, by comparing the AE index with solutions of the Lorenz system contaminated by a colored noise term, that the first SVD component in both cases is entirely due to colored noise, while the higher-order SVD components are due to the internal, low-dimensional and chaotic dynamics. By computing cross-correlation between the first SVD component of the AE index and the index itself, they concluded that the influence of the first component is about 40 percent. Further, the first SVD component is attributed to the solar wind and is characterized as linear and stochastic, while higher SVD components are attributed to magnetospheric dynamics. In our test of determinism the data are not filtered to reduce the effect of the stochastic component on the analysis, but the results still reveal that unlike IMF B_z and solar wind velocity x-component v_x, the AE index contains components that makes it different from a high-dimensional or stochastic system.

[36] Thus, it seems firmly established that the auroral electrojet proxies exhibit an additional low-dimensional component associated with self-organization of the magnetosphere, the most prominent example being the auroral substorm. It should be stressed, however, that also for AE activity the *major* component is stochastic. *Chapman and Watkins* [2001] argue that the AE index contains information transferred from the solar wind, since it has been shown in *Freeman et al.* [2000] that power laws in burst lifetime distribution for the AL and AU indices and for the solar

wind electric field $v_x B_z$ are similar apart from a bump in the lifetime distribution which *Freeman et al.* [2000] explain as a signature of the substorm current system. This indicates that the stochastic component of the auroral electrojet activity to a great extent is a direct imprint of the solar wind turbulence. This conclusion is supported by the analysis in *Rypdal and Rypdal* [2011], where B_z and tAE are found to exhibit very similar multifractal spectrum on the timescale up to 100 min.

[37] Our analysis supports a picture where the magnetosphere under quiet conditions resides in a forced state where the organization of the magnetospheric dynamics reflects the organization of the solar wind driver, i.e. the stochastic properties of the global magnetospheric system and the driver are very similar. If substorms are trigged by solar wind features, this trigger does not increase the organization or predictability of the solar wind dynamics. During substorms geomagnetic indices are influenced by a self-organization that involves the major current systems in the magnetosphere-ionosphere, and hence indicates that a global instability is exited. This picture is consistent with the scenario described in *Chang* [1999], and conceptually simpler forerunners like *Lewis* [1991]. The latter sets out to explain the unpredictability of substorm onset, noting that external triggers, like reversal from northward to southward pointing B_z, are not always identifiable, and series of substorm cycles can occur if southward IMF persists for prolonged times. Further, this picture agrees with *Klimas et al.* [2000] who simulated a spatiotemporal chaotic system that could display multiple dissipation events under constant driver. Southward IMF opens up for loading of magnetic flux and energy to the magnetosphere, and in *Lewis* [1991], and further elaborated by *Sitnov et al.* [2001], parameters representing this loading are modeled as external time-dependent control parameters, and the magnetospheric state-variable (e.g. a geomagnetic index) is modeled via a non-autonomous system of the form

$$\frac{dX}{dt} = F(X, a, b), \tag{9}$$

where $a(t)$, $b(t)$ are two time-dependent external control parameters. The underlying assumption is that the magnetosphere resides in a forced equilibrium corresponding to a stable fixed point of this system, and hence these equilibria are located on the surface $F(X, a, b) = 0$ in the three-dimensional (X, a, b)-space. Choosing a third-order polynomial form, e.g. $F(X, a, b) = X^3 + aX + b$, gives rise to a folded surface that opens the possibility of a cusp catastrophe which is interpreted as the substorm onset (expansion phase). According to this non-autonomous model for the evolution of the stable, forced equilibria, the substorm onset is not really unpredictable since it depends on the control parameters a and b. However, the catastrophe can occur along a curve in the (a, b)-plane which may be hard to identify from this kind of conceptual model, and hence practical prediction may be difficult.

[38] One unsatisfactory feature of non-autonomous models of this kind is that the control parameters are not directly related to the state of the solar wind driver, but rather a result of the solar wind/magnetosphere interaction that is an integral part of the dynamical system to be modeled. Thus, in this respect a more satisfactory approach is to model the magnetosphere-ionosphere as a dynamical system which is autonomous under constant forcing. Such models can be constructed with varying degree of sophistication [*Baker et al.*, 1990; *Klimas et al.*, 1992; *Horton and Doxas*, 1998], and may give rise to chaotic signals that reproduce many of the random characteristics of the magnetospheric time series. However, being deterministic and low-dimensional they cannot reproduce the strong stochastic component in the observational signals. On the other hand, such models can be generalized to include stochastic forcing from small-scale internal dynamics and deterministic and stochastic forcing from variations of the driver. Thus, one may conceive complicated as well as simple conceptual dynamic-stochastic models that can capture the essential stochastic dynamics as it presents itself in the observables studied here. In *Rypdal and Rypdal* [2010, 2011] the AE index is modeled by a simple dynamic-stochastic equation that reproduces the general statistical features. The deterministic dynamics in this equation was represented by a drift term (a nonlinear damping) which prevents the solution to drift off to infinity, but the focus in those studies was on the timescales less than a 100 min, where the effect of the drift term is small. A version of this stochastic difference equation that exhibits on-off intermittency for certain choices of parameters is

$$\delta X = M(x)\delta t + \sqrt{D} X\, w \tag{10}$$

where $M(x) = aX - X^3$ with $a > 0$ models the drift term found from the AE index in *Rypdal and Rypdal* [2011]. Here δt is the discrete time step (the sampling interval of the time series) and $\delta X(t) = X(t + \delta t) - X(t)$. In *Rypdal and Rypdal* [2010] $w(t)$ is modeled as a particular multifractal stochastic noise process with unit variance. It was shown by *Aumaitre et al.* [2005] that the on-off intermittency of this equation is sensitive to the nature of the noise term. If $w(t)$ is approximated by a white Gaussian noise, equation (10) in the limit $\delta \to 0$ reduces to the Itô stochastic differential equation

$$dX = \left(aX - X^3\right) dt + \sqrt{D}\, X dB(t),$$

where $B(t)$ is the Wiener process (Brownian motion). It can be shown from the associated Fokker-Planck equation that the stationary probability density for X is $P(X) = CX^{(2a/D)-1} e^{-(X^2/D)}$. The divergence of $P(X)$ as $X \to 0$ for $2a/D < 1$ is due to the on-off intermittency in this regime, which makes the solution reside in the vicinity of $X = 0$ for a considerable portion of the time, while for $2a/D - 1$ small, but positive, the solution has an intermittent character more similar to the behavior of the AE index. Such a solution, for D = 0.1, is shown in Figure 9a, with a sample of the AE index shown in Figure 9b. Here w was chosen as a weakly anti-persistent fractional Gaussian noise with Hurst exponent $H = 0.45$, which is the H-value derived from the power spectral density for AE shown in Figure 10. The relation between the spectral index β, which is the slope of the straight lines fitted to the spectra plotted in a log-log plot, and the Hurst exponent of the differentiated signal is $\beta = 2H + 1$. On timescales <100 time steps (minutes) AE index has $\beta \approx 1.90$, corresponding to $H \approx 0.45$. The power spectral density for the model signal shows a less clear power law regime on these timescales, which is

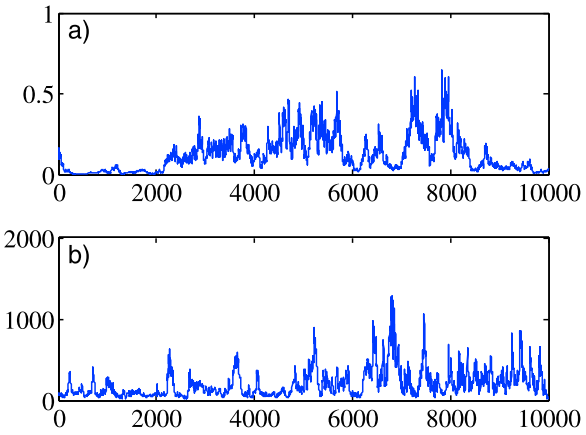

Figure 9. (a) Numerical solutions of equation (10) and (b) AE index.

mainly due to a crude model for the nonlinear drift term $M(X)$ in equation (10). A more "box-like" function would remedy this. On timescales >100 minutes the spectrum for the AE index has a pink-noise character ($\beta \approx 1$), while the model time series has a more gradual transition toward white noise. Further study on refinements of equation (10) is required to settle whether these spectral features are possible to reproduce within this class of one-dimensional stochastic equations.

[39] An interesting question is whether modeling along these lines can produce bursts (substorms) which enhance the determinism compared to a completely random process. As discussed before, the test based on comparing the L_n-curve with the one obtained after randomization of phases is a test on the existence of a low-dimensional and nonlinear component in the dynamics. Direct computation of L_n from the model signal, when $\tau = 10$ and $m = 8$, does not reveal a significant reduction of L_n after randomization, in contrast to what was found from the MG system signal in Figure 2a. One obvious reason for this is that the signal from equation (10) contains a strong stochastic component which is not present in the signal from the MG system. Hence, in this case it is necessary to perform a mild low-pass filtering of the model

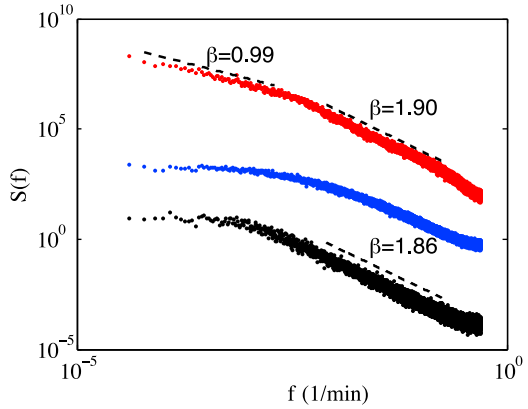

Figure 10. Power spectral densities. Top curve is from AE index. Middle curve is from solutions of equation (10) with w a fractional Gaussian noise with $H = 0.45$. Bottom curve is from O-U process with w the same as above.

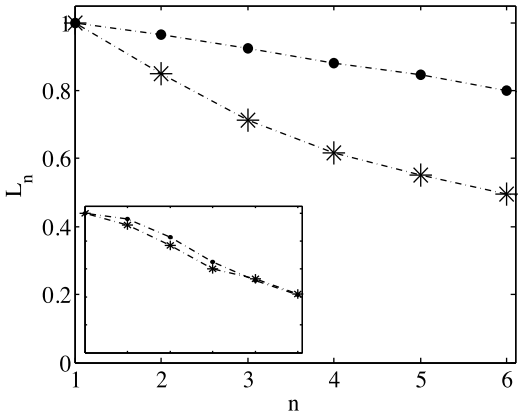

Figure 11. L_n averaged over an ensemble of realization; bullets are derived from low-pass filtered numerical solutions to equation (10), stars are derived from these solutions after randomization of phases of Fourier coefficients. Inset shows same characteristics for the filtered O-U process. Standard errors are of the same order as the symbol size.

signal before computation of L_n [*Kaplan and Glass*, 1993]. The result after filtering is shown in Figure 11, indicating the presence of a low-dimensional nonlinear component. To make sure that this filtering does not introduce spurious low-dimensional nonlinearities in the signal, we perform the same test to a filtered O-U process with similar spectral characteristics as our model signal (the power spectral density for the O-U signal is displayed in Figure 10). The filtered O-U process shows very small change of L_n after randomization of phases, as shown in the inset of Figure 11. Obviously, low-pass filtering also has an effect on this test when applied to physical signals with a stochastic component. In Figure 12 we show the effect of applying the same filter to tAE, which should be compared to the result for the unfiltered signal shown in Figure 6a.

[40] The nonlinearity producing determinism in the model signal from equation (10) is a combination of the nonlinear drift term and the multiplicative noise term $\sqrt{D}Xw$. The multiplicative term can be eliminated by the transformation

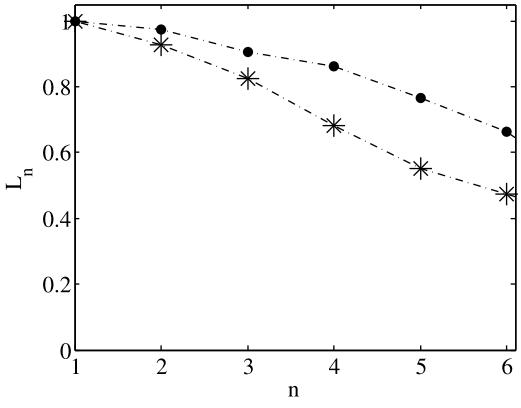

Figure 12. L_n averaged over an ensemble of realization; bullets are derived from the all low-pass filtered tAE time series, stars from this time series after randomization of phases of the Fourier coefficients. Standard errors are of the same order as the symbol size.

$Y = \log X$, but then Itô's formula [*Gardiner*, 1985] yields a new drift term on the form $\tilde{M}(Y) = e^{-Y}M(e^{Y}) - D/2$. Note that if our original drift term is a linear damping $M(X) = -\nu X$ the transformed drift term reduces to a negative constant $\tilde{M}(Y) = -(\nu + D/2)$. This yields $Y(t) \to -\infty$, and hence $X(t) \to 0$ as $t \to \infty$, and demonstrates that the drift term must be nonlinear to produce stationary time series from a model with a multiplicative noise term like equation (10).

[41] **Acknowledgments.** The authors acknowledge extensive discussions with M. Rypdal. Recurrence plot and the longest diagonal line are computed by means of the Matlab package downloaded from http://www.agnld.uni-potsdam.de/marwan/toolbox/. The authors would like to thank the Kyoto World Data Center for AE, AL, AU and PC indices.

[42] Philippa Browning thanks the reviewers for their assistance in evaluating this paper.

References

Abarbanel, H. (1996), *Analysis of Observed Chaotic Data*, Springer, New York.

Athanasiu, M. A., and G. P. Pavlos (2001), SVD analysis of the magnetospheric AE index time series and comparison with low-dimensional chaotic dynamics, *Nonlinear Processes Geophys.*, *8*, 95.

Aumaitre, S., F. Pétélis, and K. Mallick (2005), Low-frequency noise controls on-off intermittency of bifurcating systems, *Phys. Rev. Lett.*, *95*, 064101.

Bak, P., C. Tang, and K. Wiesenfeld (1987), Self-organized criticality: An explanation of 1/f noise, *Phys. Rev. Lett.*, *59*, 381.

Baker, D. N., A. J. Klimas, R. L. McPherron, and J. Büchner (1990), The evolution from weak to strong geomagnetic activity: An interpretation in terms of deterministic chaos, *Geophys. Res. Lett*, *17*, 41.

Chang, T. S. (1999), Self-organized criticality, multi-fractal spectra, sporadic localized reconnections and intermittent turbulence in the magnetotail, *Phys. Plasmas*, *6*, 4137.

Chapman, S., and N. Watkins (2001), Avalanching and self-organised criticality, a paradigm for geomagnetic activity, *Space Sci. Rev.*, *95*, 293.

Chapman, S. C., N. W. Watkins, R. O. Dendy, P. Helander, and G. Rowlands (1998), A simple avalanche model as an analogue for magnetospheric activity, *Geophys. Res. Lett.*, *25*, 2397.

Davies, T. N., and M. Sugiura (1966), Auroral electrojet activity index AE and its universal time variations, *J. Geophys. Res.*, *71*, 785.

Eckmann, J. P., S. O. Kamphorst, and D. Ruelle (1987), Recurrence plots of dynamical systems, *Europhys. Lett.*, *5*, 973.

Feldstein, Y. I., V. A. Popov, J. A. Cumnock, A. Prigancova, L. G. Bloomberg, J. U. Kozyra, B. T. Tsurutanj, L. I. Gromova, and A. E. Levitin (2006), Auroral electrojets and boundaries of plasma domains in the magnetosphere during magnetically disturbed intervals, *Ann. Geophys.*, *24*, 2243.

Freeman, M. P., N. W. Watkins, and D. J. Riley (2000), Evidence for a solar wind origin of the power law burst lifetime distribution of the AE indices, *Geophys. Res. Lett.*, *27*, 1087.

Frey, H. U., S. B. Mende, V. Angelopoulos, and E. F. Donovan (2004), Substorm onset observations by IMAGE-FUV, *J. Geophys. Res.*, *109*, A10304, doi:10.1029/2004JA010607.

Gardiner, C. W. (1985), *Handbook of Stochastic Methods*, Springer, New York.

Golovchanskaya, I. V., B. V. Kozelov, T. I. Sergienko, U. Brändström, H. Nilsson, and I. Sandahl (2008), Scaling behavior of auroral luminosity fluctuations observed by Auroral Large Imaging System (ALIS), *J. Geophys. Res.*, *113*, A10303, doi:10.1029/2008JA013217.

Horton, W., and I. Doxas (1998), A low-dimensional dynamical model for the solar wind driven geotail-ionosphere system, *J. Geophys. Res.*, *103*, 4561.

Kaplan, D. T., and L. Glass (1992), Direct test for determinism in a time series, *Phys. Rev. Lett.*, *68*, 427.

Kaplan, D. T., and L. Glass (1993), Coarse-grained embedding of time series: Random walks, Gaussian random processes, and deterministic chaos, *Physica D*, *64*, 431.

Klimas, A. J., D. N. Baker, D. A. Roberts, D. H. Fairfield, and J. Büchner (1992), A nonlinear dynamical analogue model of geomagnetic activity, *J. Geophys. Res.*, *97*, 12,253.

Klimas, A., J. A. Valdivia, D. Vassiliadis, J. Takalo, and D. Baker (2000), Self-organized criticality in the substorm phenomenon and its relation to localized reconnection in the magnetospheric plasma sheet, *J. Geophys. Res.*, *105*, 18,765.

Kozelov, B. V., and T. V. Kozelova (2003), Cellular automata model of magnetospheric-ionospheric coupling, *Ann. Geophys.*, *21*, 1931.

Lewis, Z. V. (1991), On the apparent randomness of substorm onset, *Geophys. Res. Lett.*, *18*, 1627.

Mackey, M. C., and L. Glass (1977), Oscillation and chaos in physiological control systems, *Science*, *197*, 197.

March, T. K., S. C. Chapman, and R. O. Dendy (2005a), Recurrence plot statistics and the effect of embedding, *Physica D*, *200*, 171.

March, T. K., S. C. Chapman, and R. O. Dendy (2005b), Mutual information between geomagnetic indices and the solar wind as seen by WIND: Implications for propagation time estimates, *Geophys. Res. Lett.*, *32*, L04101, doi:10.1029/2004GL021677.

Marwan, N., M. C. Romano, M. Thiel, and J. Kűrths (2007), Recurrence plots for the analysis of complex systems, *Phys. Rep.*, *438*, 237.

Marwan, N., et al. (2008), 20 years of recurrence plots: Perspectives for a multi-purpose tool of nonlinear data analysis, *Eur. Phys. J. Spec. Top.*, *164*, 3.

Rypdal, M., and K. Rypdal (2010), Stochastic modeling of the AE index and its relation to fluctuations in B_z of the IMF on time scales shorter than substorm duration, *J. Geophys. Res.*, *115*, A11216, doi:10.1029/2010JA015463.

Rypdal, M., and K. Rypdal (2011), Discerning a linkage between solar wind turbulence and ionospheric dissipation by a method of confined multifractal motions, *J. Geophys. Res.*, *116*, A02202, doi:10.1029/2010JA015907.

Sharma, A. S., D. Vassiliadis, and K. Papadopoulos (1993), Reconstruction of low-dimensional magnetospheric dynamics by singular spectrum analysis, *Geophys. Res. Lett.*, *20*, 335.

Sitnov, M. I., A. S. Sharma, and K. Papadopoulos (2001), Modeling substorm dynamics of the magnetosphere: From self-organization and self-organized criticality to nonequlibrium phase transitions, *Phys. Rev. E*, *65*, 016116.

Takens, F. (1981), Detecting strange attractors in fluid turbulence, in *Dynamical Systems and Turbulence*, edited by D. Rand and L. S. Young, *Lect. Notes Math.*, *898*, 366.

Trulla, L. L., A. Guliani, J. P. Zbilut, and C. L. Webber Jr. (1996), Recurrence quantification analysis of the logisitc equation with transients, *Phys. Lett. A*, *223*, 255.

Tsurutani, B., M. Sugiura, and T. Iyemori (1990), The nonlinear response of AE to the IMF B_s driver: A spectral break at 5 h, *Geophys. Res. Lett.*, *17*, 279.

Uritsky, V. M., and M. I. Pudovkin (1998), Low frequency 1/f-like fluctuations of the AE-index as a possible manifestation of self-organized criticality in the magnetosphere, *Ann. Geophys.*, *16*, 1580.

Uritsky, V. M., A. J. Kimas, and D. Vassiliadis (2002), Multiscale dynamics and robust critical scaling in a continuum current sheet model, *Phys. Rev. E*, *65*, 046113.

Valdivia, J. A., D. Vassiliadis, and A. Klimas (1999), Modeling the spatial structure of the high latitude magnetic perturbations and the related current systems, *Phys. Plasmas*, *6*, 4185.

Valdivia, J. A., J. Rogan, V. Munoz, and B. Toledo (2006), Hysteresis provides self-organization in a plasma model, *Space Sci. Rev.*, *122*, 313, doi:10.7007/s11214-00607846-2.

Vennestrøm, S., E. Friis-Christensen, O. A. Troshichev, and V. G. Andrezen (1991), Comparison between the polar cap PC and the auroral electrojet indices AE, AL and AU, *J. Geophys. Res.*, *96*, 101.

Vörös, Z. (1991), Synergetic approach to substorm phenomenon, in *Magnetospheric Substorms*, *Geophys. Monogr. Ser.*, vol. 64, edited by J. R. Kan, p. 461, AGU, Washington, D. C.

Wanliss, J. A., and K. M. Showalter (2006), High-resolution global storm index: *Dst* versus SYM-H, *J. Geophys. Res.*, *111*, A02202, doi:10.1029/2005JA011034.

Webber, C. L., Jr., and J. P. Zbilut (1994), Dynamical assessment of physiological systems and states using recurrence plot strategies, *J. App. Phys.*, *76*, 965.

Živković, T., and K. Rypdal (2011), Low-dimensionality and predictability of solar wind and global magnetosphere during magnetic storms, *J. Geophys. Res.*, *116*, A10215, doi:10.1029/2011JA016547.